Haskell N. A. (1964). Total energy spectral density of elastic wave radiation from propagating faults, Bull. Seism. Soc. Am. **54**, 1811–1841

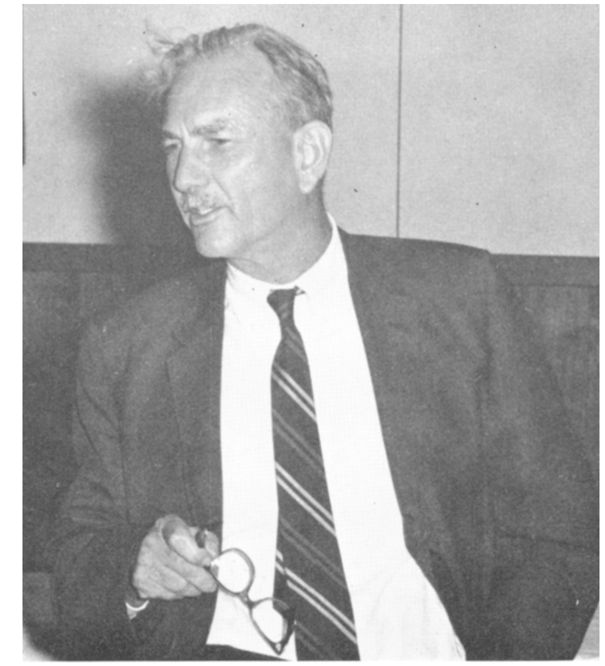

NORMAN A. HASKELL

Rupture →

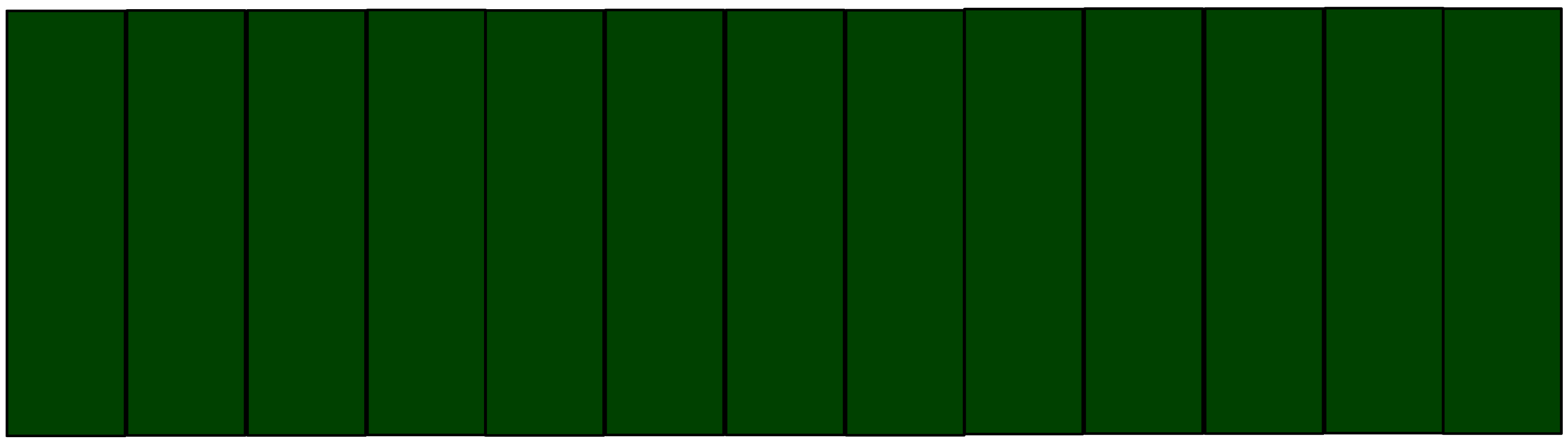

Sumatra earthquake, Dec 26, 2004

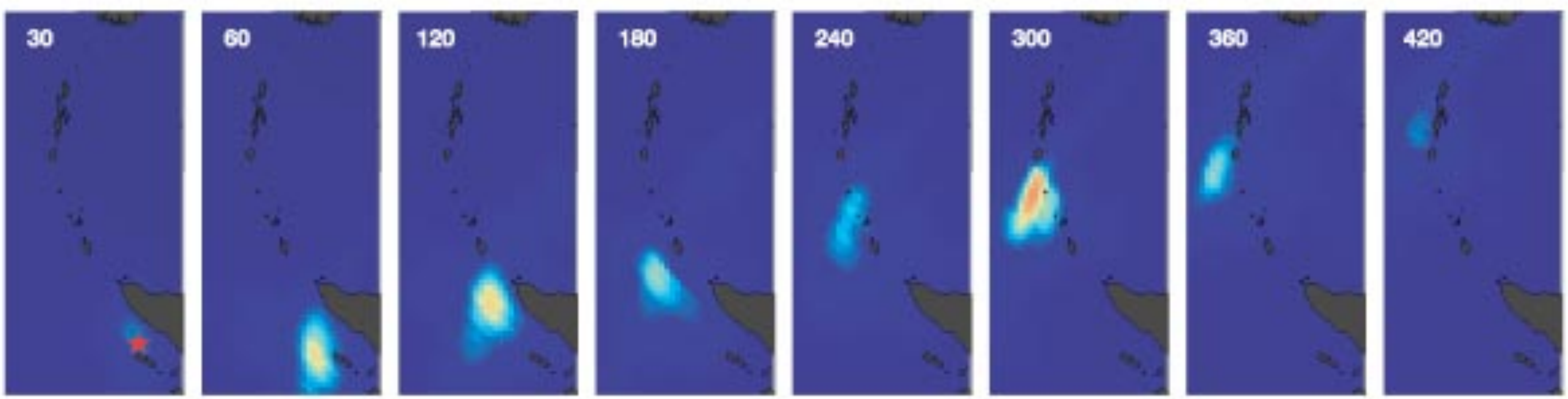

Ishii et al., Nature 2005 doi:10.1038/nature03675

Haskell source model: far field

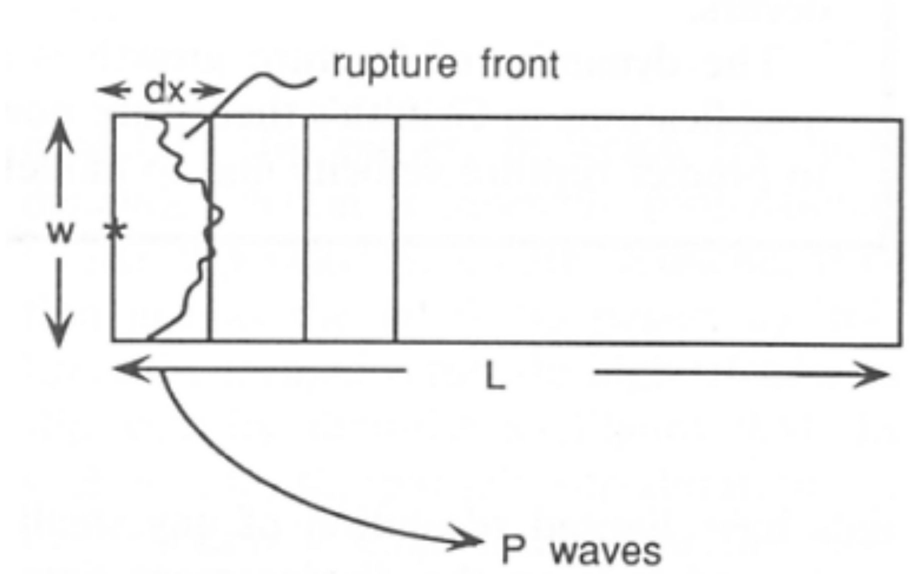

FIGURE 9.5 Geometry of a one-dimensional fault of width *w* and length *L*. The individual segments of the fault are of length *dx*, and the moment of a segment is *m dx*. The fault ruptures with velocity v_r.

$$u_r(r,t) = \sum_{i=1}^{N} u_i\left(r_i, t - r_i/\alpha - \Delta t_i\right) =$$

$$= \frac{R_i^P \mu}{4\pi\rho\alpha^3} W \sum_{i=1}^{N} \frac{\dot{D}_i}{r_i}\left(t - \Delta t_i\right) dx \approx$$

$$\approx \frac{R_i^P \mu}{4\pi\rho\alpha^3} \frac{W}{r} \sum_{i=1}^{N} \dot{D}(t) * \delta\left(t - \frac{x}{v_r}\right) dx \approx$$

$$\approx \frac{R_i^P \mu}{4\pi\rho\alpha^3} \frac{W}{r} \dot{D}(t) * \int_0^L \delta\left(t - \frac{x}{v_r}\right) dx =$$

$$= \frac{R_i^P \mu}{4\pi\rho\alpha^3} \frac{W}{r} v_r \dot{D}(t) * B(t; T_r)$$

Haskell source model: far field

$$u_r(r,t) \propto \dot{D}(t) * v_r H(z)\Big|_{t-x/v_r}^{t} = v_r \dot{D}(t) * B(t;T_r)$$

resulting in the convolution of two boxcars: the first with duration equal to the rise time and the second with duration equal to the **rupture time** (L/v_r)

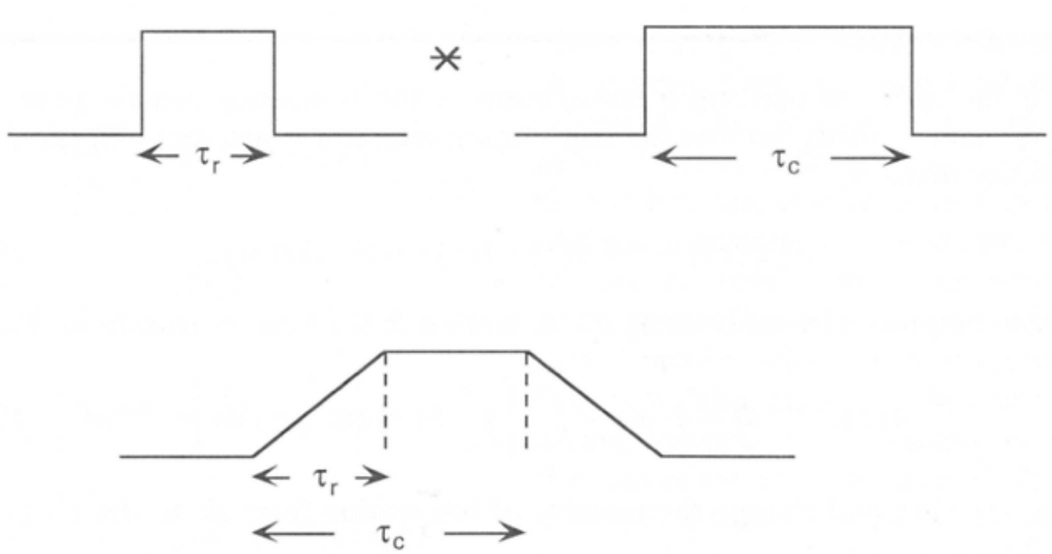

FIGURE 9.6 The convolution of two boxcars, one of length τ_r and the other of length τ_c ($\tau_c > \tau_r$). The result is a trapezoid with a rise time of τ_r, a top of length $\tau_c - \tau_r$, and a fall of width τ_r.

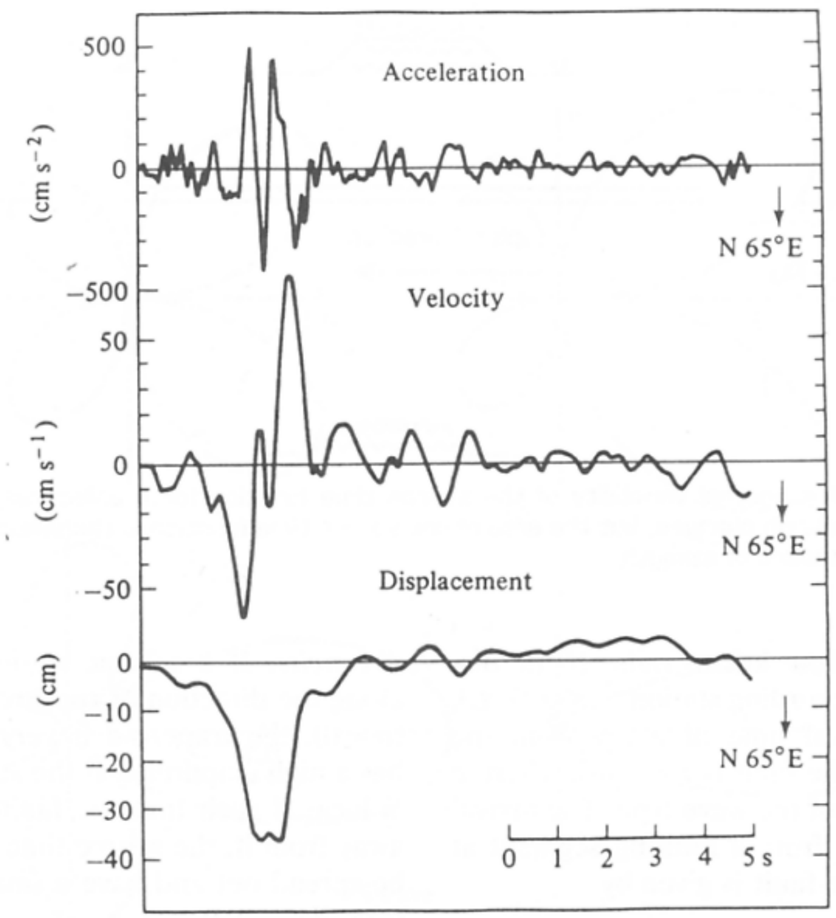

FIGURE 9.7 A recording of the ground motion near the epicenter of an earthquake at Parkfield, California. The station is located on a node for *P* waves and a maximum for *SH*. The displacement pulse is the *SH* wave. Note the trapezoidal shape. (From Aki, *J. Geophys. Res.* 73, 5359–5375, 1968; © copyright by the American Geophysical Union.)

Haskell source model: directivity

The body waves generated from a breaking segment will arrive at a receiver before than those that are radiated by a segment that ruptures later.

If the path to the station is not perpendicular, the waves generated by different segments will have different path lengths, and then unequal travel times.

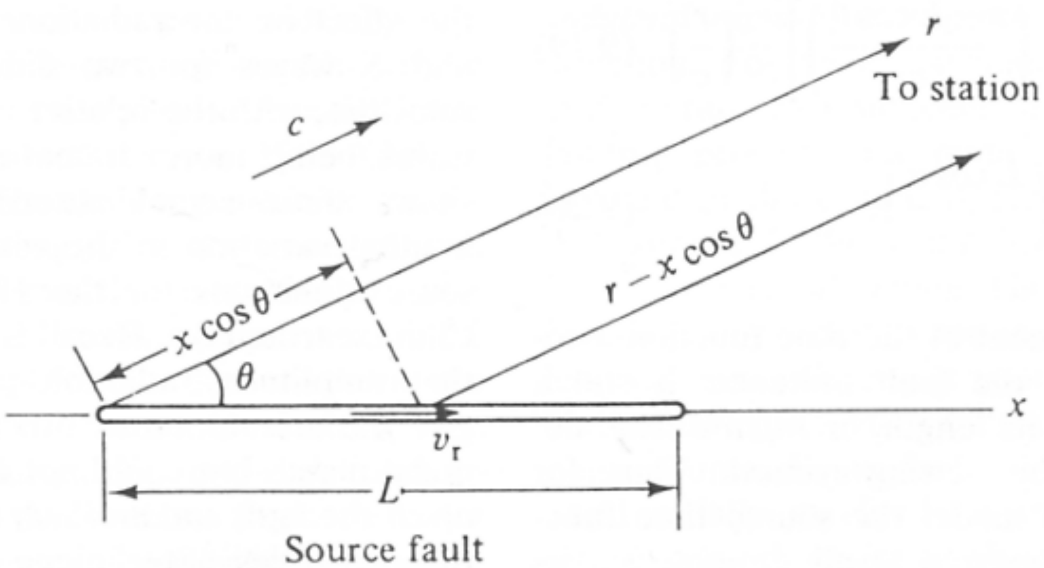

FIGURE 9.8 Geometry of a rupturing fault and the path to a remote recording station. (From Kasahara, 1981.)

$$T_r = \left[\frac{L}{v_r} + \left(\frac{r - L\cos\theta}{c}\right)\right] - \frac{r}{c} =$$

$$= \frac{L}{v_r} - \left(\frac{L\cos\theta}{c}\right) = \frac{L}{v_r}\left(1 - \frac{v_r}{c}\cos\theta\right)$$

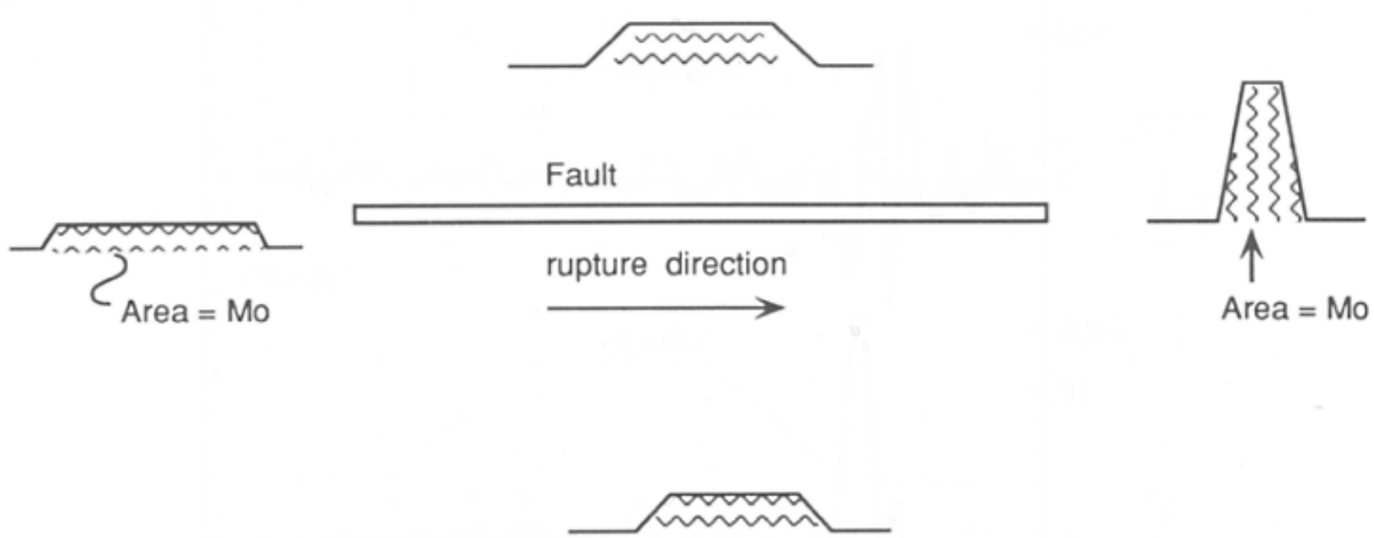

FIGURE 9.9 Azimuthal variability of the source time function for a unilaterally rupturing fault. The duration changes, but the area of the source time function is the seismic moment and is independent of azimuth.

Rupture velocity

Earthquake ruptures typically propagate at velocities that are in the range 70–90% of the S-wave velocity and this is independent of earthquake size. A small subset of earthquake ruptures appear to have propagated at speeds greater than the S-wave velocity. These supershear earthquakes have all been observed during large strike-slip events.

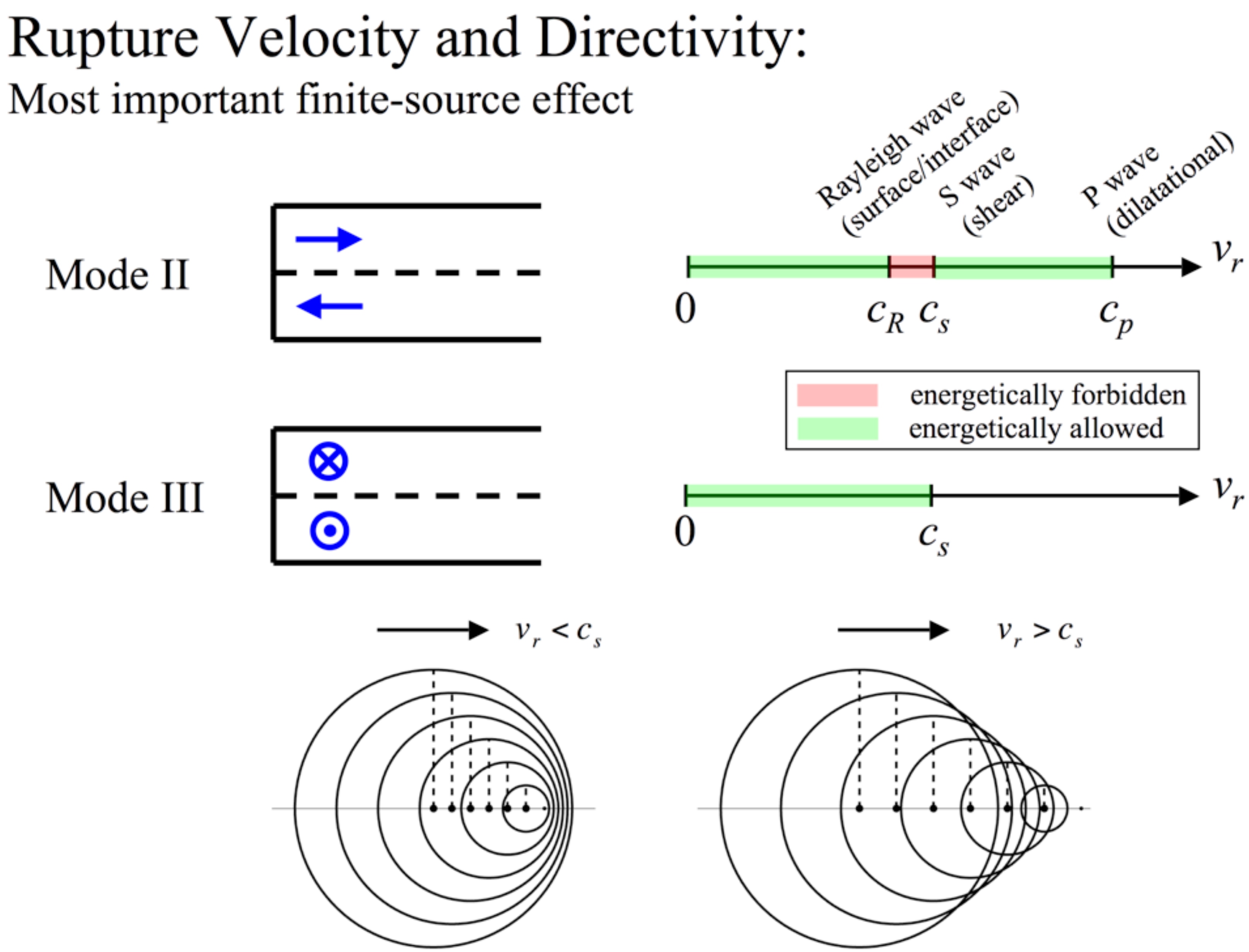

http://pangea.stanford.edu/~edunham/research/supershear.html

Directivity example

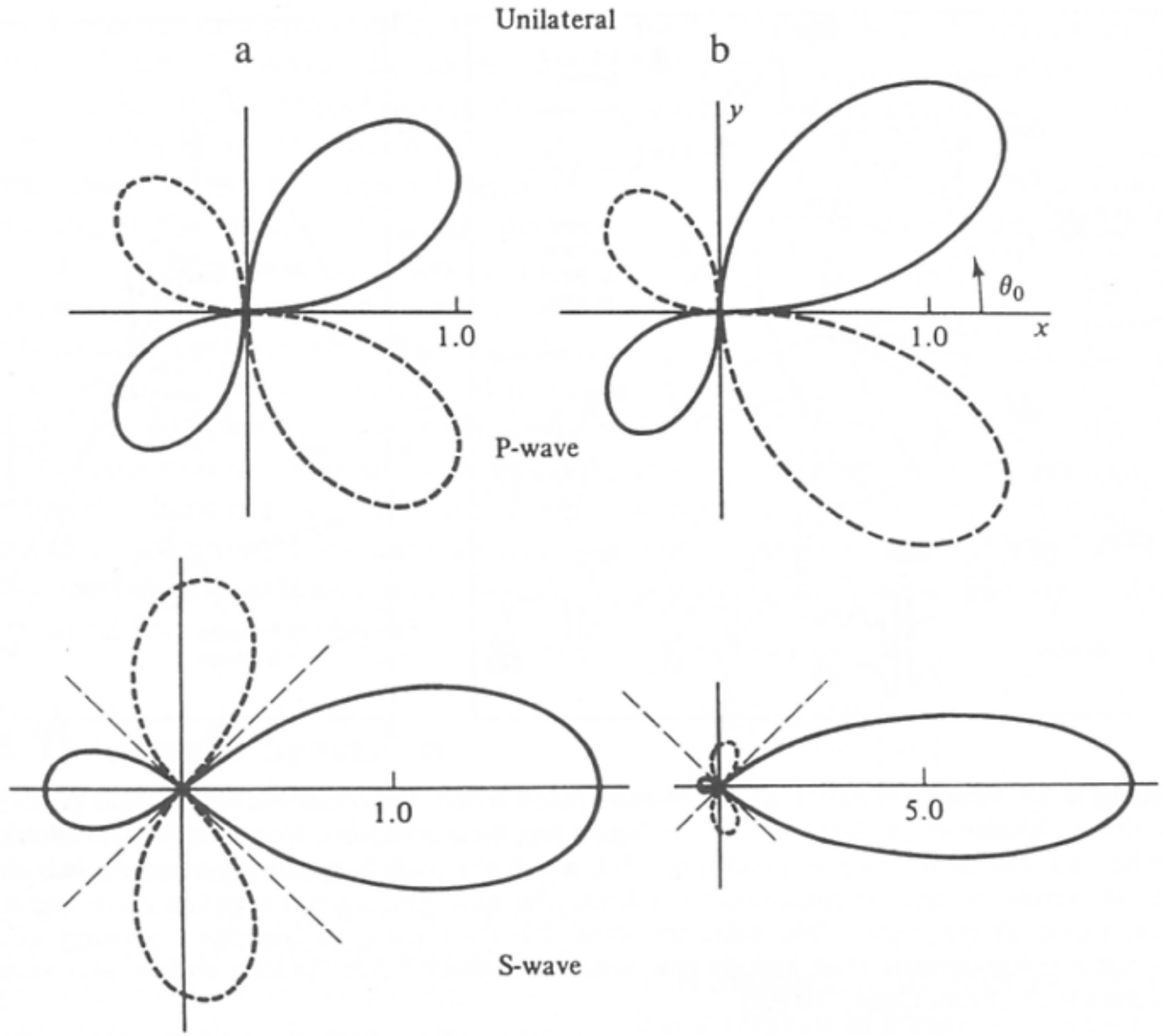

FIGURE 9.10 The variability of *P*- and *SH*-wave amplitude for a propagating fault (from left to right). For the column on the left $v_r/v_s = 0.5$, while for the column on the right $v_r/v_s = 0.9$. Note that the effects are amplified as rupture velocity approaches the propagation velocity. (From Kasahara, 1981.)

Source spectrum

The displacement pulse, corrected for the geometrical spreading and the radiation pattern can be written as:

$$u(t) = M_0 \left[B\left(t;\tau\right) * B\left(t;T_R\right) \right]$$

and in the frequency domain:

$$\left|U\left(\omega\right)\right| = M_0 \left|F\left(\omega\right)\right| = M_0 \left| \frac{\sin\left(\frac{\omega\tau}{2}\right)}{\left(\frac{\omega\tau}{2}\right)} \right| \left| \frac{\sin\left(\frac{\omega L}{v_r 2}\right)}{\left(\frac{\omega L}{v_r 2}\right)} \right| \approx \begin{cases} M_0 & \omega < \frac{2}{T_r} \\ \frac{2M_0}{\omega T_R} & \frac{2}{T_r} < \omega < \frac{2}{\tau} \\ \frac{4M_0}{\omega^2 \tau T_R} & \omega > \frac{2}{\tau} \end{cases}$$

Source spectrum (amplitude)

$$U(\omega) \approx \begin{cases} M_0 & \omega < \dfrac{2}{T_r} \\[2ex] \dfrac{2M_0}{\omega T_R} & \dfrac{2}{T_r} < \omega < \dfrac{2}{\tau} \\[2ex] \dfrac{4M_0}{\omega^2 \tau T_R} & \omega > \dfrac{2}{\tau} \end{cases}$$

Figure 4.6-4: Approximation of the (sin *x*)/*x* function, and derivation of corner frequencies.